Control of skyrmion magnetic bubble gyration

Kyoung-Woong Moon,[1] Byong Sun Chun,[1] Wondong Kim,[1] Z. Q. Qiu,[2] and Chanyong Hwang[1,*]
[1]*Center for Nanometrology, Korea Research Institute of Standards and Science, Daejeon 305-340, Republic of Korea*
[2]*Physics Department, University of California at Berkeley, Berkeley, California 94720, USA*
(Received 2 August 2013; revised manuscript received 3 December 2013; published 18 February 2014)

The skyrmion magnetic bubble in a ferromagnetic disk exhibits hypocycloidal gyrations contrary to the vortex gyration, showing a simple circular trajectory. To describe the hypocycloidal bubble gyration, a mass term is needed in Thiele's equation. In this study, we analytically derived both mass and spring constant term, which are crucial parameters for describing the bubble gyration. Values obtained by these analytic expressions were consistent with those obtained by simulations. We could find the dependences of these two terms on several external parameters, including the bubble radius. Especially using the radius's dependence, we could obtain regular polygonlike trajectories such as a square and a triangle confirmed by the numerical simulations. Based on this effective method to control the bubble gyration, the regular polygonlike trajectories of this skyrmion magnetic bubble make it possible to study the bubble gyration without time-resolved experiments.

DOI: 10.1103/PhysRevB.89.064413 PACS number(s): 75.70.Kw, 75.78.Cd, 75.75.Fk, 12.39.Dc

I. INTRODUCTION

The dynamics of a magnetic vortex has been one of the major issues in magnetism because of its interesting physics and possibilities for applications [1–6]. The magnetic vortex is a fundamental state in the soft magnetic disks and is comprised typically by the vortex core, which has magnetization points out of the plane and is surrounded by chiral in-plane magnetizations. The dynamics of the position of vortex core $\mathbf{R}$ in a parabolic potential well is described by Thiele's equation as [7,8]

$$\mathbf{G} \times \dot{\mathbf{R}} - \mathcal{K}\mathbf{R} - D\dot{\mathbf{R}} = 0. \tag{1}$$

Here, $\mathbf{G}$ is a gyrocoupling vector, $\mathcal{K}$ denotes a spring constant for a restoring force induced by the parabolic potential well, $U(X,Y) = \mathcal{K}(X^2 + Y^2)/2$, and D is a dissipation tensor. Among these three coefficients, $\mathbf{G}$ is the most important for gyration because the rotation of the core is induced by $\mathbf{G}$. If we set the z axis perpendicular to the disk plane, $\mathbf{G} = (0, 0, \mathcal{G})$, where $\mathcal{G} = -4\pi qdM/\gamma$, d is the disk thickness, M is the magnetization, and γ is the gyromagnetic ratio, q is the skyrmion charge and is determined by $q = (1/4\pi)\int dxdy\mathbf{m} \cdot (\partial_x\mathbf{m} \times \partial_y\mathbf{m})$ with the normalized magnetization $\mathbf{m}$ [9]. The vortex is known to have $q = \pm 1/2$, so gyration of the vortex core is expected because of the nonzero $\mathbf{G}$ [3,9].

Equation (1) describes successfully the vortex core motion in in-plane magnetization disks, and many experiments have been carried out based on Eq. (1) [1,2,4]. As a result, the vortex state and its related dynamics are understood both theoretically and experimentally. A question of what would be the corresponding state in perpendicular magnetization anisotropy disks was asked [10], and the answer is a magnetic bubble state.

The magnetic bubble state [10–14] is a circular domain placed in the center of the disk and surrounded by the domain with an opposite magnetization, as shown in Fig. 1(a). Inner and outer domains have perpendicular magnetization due to the strong perpendicular magnetic anisotropy. Between the two domains, the magnetization direction rotates gradually from one to the other direction, forming a domain wall. This bubble state was also expected to exhibit a circular gyration like a vortex core because the bubble state has nonzero skyrmion charge $q = \pm 1$ [10,15,16].

However, Moutafis *et al.* showed that the skyrmion magnetic bubble rotation does not follow Eq. (1). Through numerical simulations, they showed that the trajectory of the bubble rotation roughly resembles a pentagon, not a circle [15]. This unconventional trajectory has been a problem of the dynamical motion of a skyrmion bubble. Recently, Makhfudz *et al.* have finally solved this mysterious trajectory [16]. They inserted a Newtonian mass term in Thiele's equation as

$$\mathbf{G} \times \dot{\mathbf{R}} - \mathcal{K}\mathbf{R} - D\dot{\mathbf{R}} = \mathcal{M}\ddot{\mathbf{R}}. \tag{2}$$

Then, Eq. (2) exactly describes the skyrmion bubble trajectory. Equation (2) produces two different frequencies with opposite signs, meaning that two waves with opposite directions propagate along the domain wall, and their combined motion generates a hypocycloid trajectory that has been called "roughly a pentagon."

In this report, we focused on questions such as the following. How can we get "a regular pentagon" trajectory? How can we obtain regular polygonlike trajectories having a natural number of vertices during one rotation such as a triangle and a square? We suggest an effective method for obtaining a regular polygon trajectory. Regular polygon trajectories are useful for experiments aimed at detecting the bubble gyrations. In addition, we also provide the analytic expression for the spring constant and the mass constant induced by the dipolar repulsion. These analytic expressions are useful to expect the skyrmion bubble gyration and further studies including the Dzyaloshinsky-Moriya interaction (DMI) [3,17,18].

II. MICROMAGNETIC SIMULATIONS

A "regular pentagon" trajectory that has five vertices is shown in Fig. 1(b), which was generated by a simulation similar to that of Moutafis *et al.* [15]. The significant difference between the two simulations is an external field in the z direction. We applied the nonzero external field -7 mT along

*Corresponding author: cyhwang@kriss.re.kr

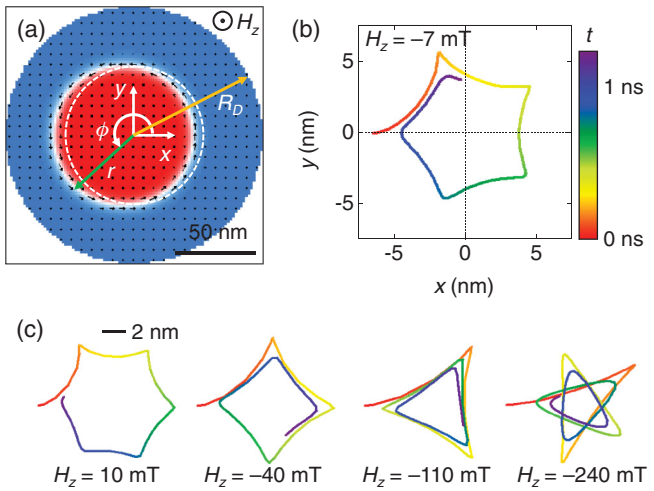

FIG. 1. (Color online) (a) A skyrmion magnetic bubble domain state in a perpendicular magnetic anisotropy disk. The magnetization of the bubble is aligned in the $-z$ direction (colored red). The blue color represents alignment of the magnetization in the $+z$ direction. Black arrows in the disk denote the in-plane magnetization direction. A white dashed circle represents the domain wall position where the total energy is minimized. The bubble position shifted −6.4 nm from the white dashed circle to the x direction for gyration. (b) A regular pentagonlike trajectory of the bubble domain gyration with the external field $H_z = -7$ mT. The line represents the trajectory of the center of the bubble. The trajectory has five vertices and thus resembles a regular pentagon. (c) Several examples of regular polygonlike trajectory with respect to the external field. The time scale is the same as in (b).

the z axis. The other parameters were set to the same values as Moutafis' simulations. The saturation magnetization was set at $M = 10^6$ A/m, the exchange stiffness at $A = 1.0 \times 10^{-11}$ J/m, and the uniaxial anisotropy along the z direction for perpendicular magnetization at $K = 1.3 \times 10^6$ J/m^3. The disk was 160 nm ($=2R_D$) in diameter and 32 nm in thickness. We divided the structure on the x-y plane by 1.6 nm × 1.6 nm cells and assumed uniform magnetization along the thickness direction. The damping constant $\alpha = 0.01$ was used. The simulations were carried out by the object-oriented micromagnetic framework (OOMMF) simulator [19] without DMI [20]. To obtain the "regular pentagon" trajectory, before starting the gyration, an external field H_z in the z direction was applied until the magnetization state was stabilized, and then the bubble position shifted to the x direction with −6.4 nm distance. To shift the bubble position, the magnetization of each cell was replaced by the magnetization of four cells ahead in the x direction. Figure 1(a) shows an initial magnetization state of the shifted bubble. Next, we relaxed the magnetization state with constant H_z to keep the bubble radius constant. Note that the shifting method used in this study is different from that of Moutafis *et al*. They use the external field gradient to shift the bubble position [15]. Despite these differences, the trajectory with the zero external field was basically the same as that of the result of Moutafis *et al*. The only differences were the amplitude and start position of gyration. To draw the gyration trajectory, the center position was found by circular fittings of the domain wall position, where the perpendicular component of magnetization was 0. We obtained the domain wall distance r from the center of the disk as a function of the azimuthal angle ϕ, and then the center of the bubble was calculated by circular fitting. Thus, the trajectory shown in Fig. 1(b) represents the center of the domain wall.

In addition to a pentagon trajectory, the external field can produce a regular polygonlike trajectory. Figure 1(c) shows several examples of the trajectory: a hexagon with $H_z = 10$ mT, a square with −40 mT, and a triangle with −110 mT. When H_z decreases, the number of polygon sides and interior angles also decrease. As a result, a pentagram trajectory was obtained at $H_z = -240$ mT. From these results, we verified that the external field could determine the trajectories of bubble gyration, including regular polygonlike shapes.

III. RESULT AND DISCUSSION

Makhfudz *et al*. show that these hypocycloid trajectories are generated by two different wave modes with opposite propagation directions and different speeds [16]. The shifted initial magnetization state consisted of two sinusoidal waves with wave number $k = 1/\bar{r}$. After starting the relaxation, these two waves propagate along the domain wall with different frequencies, which can be derived from Eq. (2) by neglecting the damping term because the gyrotropic force overwhelms the viscous force:

$$\omega_{\pm} = -\frac{\mathcal{G}}{2\mathcal{M}} \pm \sqrt{\left(\frac{\mathcal{G}}{2\mathcal{M}}\right)^2 + \frac{\mathcal{K}}{\mathcal{M}}}. \tag{3}$$

These two frequencies were obtained from simulations. The value of ω_+ was obtained directly from gyration because ω_+ was related to one rotation time of the bubble; then, we could calculate ω_- from the number of polygon sides during one rotation. For example, when $H_z = -110$ mT, the number of sides of the trajectory is 3.01, and $\omega_+/2\pi = 2.21$ GHz. Then ω_- was calculated from this relation, $\omega_-/2\pi = -\omega_+/2\pi \times (N-1) = -4.43$ GHz [16], where N is the number of sides. Figure 2 shows the two frequencies with respect to the external field. ω_+ and ω_- have opposite signs, and the amount of ω_- is always larger than ω_+. The external field also changes the bubble radius. The negative field of H_z expands the radius of the bubble because the bubble has negative magnetization in the z direction. The expansion of the domain occurred until the change in Zeeman energy was compensated by the dipolar and tension energies [21]. Then, the radius had a stabilized value. The averaged radii of the bubble domain with respect to the external fields H_z are shown in the inset of Fig. 2. The bubble radius increases monotonically as H_z decreases. The bubble state persists in the external field range from −290 to 59 mT. If the external field exceeds the range, the bubble domain disappears, and the disk produces a single domain state.

According to Eq. (3), the two frequencies are determined by only three constants: the spring constant $\mathcal{K}$, the mass constant $\mathcal{M}$, and the gyrotropic constant $\mathcal{G}$. Among these constants, the gyrotropic constant is a material and structural parameter and is determined as $\mathcal{G} = -4\pi q d M/\gamma = 2.29\times 10^{-12}$ J s/m^2 in this study ($q = -1$) [16]. Thus, we should think only about the

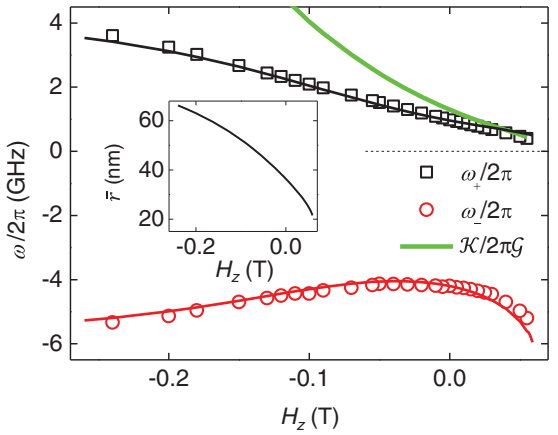

FIG. 2. (Color online) Frequencies obtained by gyration results with respect to the external magnetic field H_z applied to the perpendicular direction to the disk; ω_+ (□) is obtained by a clockwise rotation of the bubble, and ω_- (○) represents counterclockwise rotation of the bubble. The thick green line (—) denotes the frequency derived from the massless Thiele's equation. The black (—) and red (—) lines are obtained by analytic equation. The inset shows the averaged radius $\bar{r}$ as a function of H_z.

two parameters $\mathcal{K}$ and $\mathcal{M}$ to understand the physical meaning of the two frequencies. From Eq. (3), we derived the mass and the spring constant separately. By adding ω_+ and ω_-, the mass constant could be represented as follows:

$$\mathcal{M} = \frac{-\mathcal{G}}{\omega_+ + \omega_-}. \tag{4}$$

The mass constant obtained from the simulation was plotted in Fig. 3(a) as a function of the bubble radius. It is interesting to note that the mass constant was in exact linear relation with the bubble radius, and we thought that the mass of the bubble was determined by the total length of the domain wall and not by the area of the bubble. According to Makhfudz *et al.*, the mass is determined by $\mathcal{M} = \pi \bar{r} g^2/\kappa$, where $g = \mathcal{G}/2\pi$ and κ is a constant related to the domain wall energy density difference between the Bloch and Néel wall configurations [16,22,23]. Note that they pointed out the difference values of κ obtained, respectively, from simulation ($\kappa_{\rm sim} = 1.36 \times 10^{-10}$ J/m) and from calculation ($\kappa_{calc} = 2.81 \times 10^{-10}$ J/m). To solve this discrepancy, we obtained κ through the analytic approach. The energy density per unit length induced by the surface magnetic charge on the domain wall is represented as $(\mu_0/2)\, N_i^W M^2 d\lambda$. Here, λ is the domain wall width, and in this study $\lambda = 9.1$ nm. The coefficient $1/2$ means the self-energy. N_i^W is the direction-dependent ($i = r, \phi, z$) demagnetization factor of the wall. The Bloch and Néel wall sates correspond to $i = \phi$ and $i = r$, respectively, as depicted in Fig. 3(b). Then, the wall-type energy difference is defined as $\kappa = (\mu_0 M^2 d\lambda/2)(N_r^W - N_\phi^W)$ [24]. Due to the nonexistence of surface charges on the Bloch wall, N_ϕ^W is 0. For calculating N_r^W, we assumed an infinite rectangular stripe with a thickness d and a width λ and computed the dipolar field. Using the demagnetization factor N_r^W, we finally obtained the following equation describing the

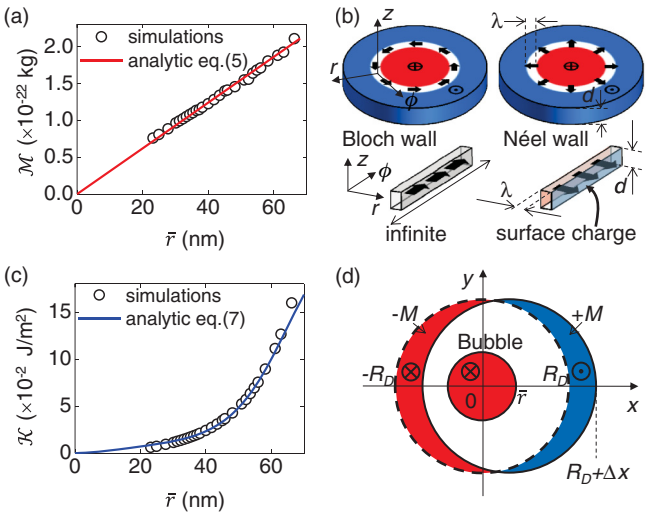

FIG. 3. (Color online) Mass constant $\mathcal{M}$ and spring constant $\mathcal{K}$ for the skyrmion bubble gyration. (a) Mass of the bubble with respect to $\bar{r}$. The line is obtained by the analytic Eq. (5). (b) Origin of the skyrmion bubble mass. The energy difference between the Bloch and Néel-type wall generates the mass of the bubble. The Bloch wall does not make any surface magnetic charge on the domain wall, but the Néel wall does. (c) The dependence of the spring constant on the bubble radius. The line is obtained by the analytic Eq. (7). (d) The schematic diagram describing the origin of the spring constant. When the disk moves from the initial position (dashed circle) to the x direction, excessive magnetic surface charges are induced.

skyrmion bubble mass:

$$\mathcal{M} \approx \frac{4\pi^2 g^2}{\mu_0 M^2 \lambda}\left[4d\tan^{-1}\left(\frac{2d}{\lambda}\right) - \lambda \ln\left(1 + \left(\frac{2d}{\lambda}\right)^2\right)\right]^{-1} \bar{r}. \tag{5}$$

From Eq. (5), κ is determined as 1.35×10^{-10} J/m, which is the same as the simulation result in Ref. [16]. We also plotted the above equation in Fig. 3(a), and we confirmed a good match between the analytic and the simulation results.

Next, we obtained the spring constant $\mathcal{K}$ from the two angular frequencies ω_+ and ω_- in Eq. (3). Then $\mathcal{K}$ could be written as

$$\mathcal{K} = \frac{\mathcal{G}\omega_+\omega_-}{\omega_+ + \omega_-}. \tag{6}$$

The spring constants calculated by Eq. (6) were plotted as points in the inset of Fig. 3(c). The parameter $\mathcal{K}$ increases exponentially as $\bar{r}$ increases. Contrary to the mass constant that exhibits clear linear relation with the bubble radius, dependence of $\mathcal{K}$ on external parameters is not simple. When the bubble moves from the disk center with the constant bubble radius, the Zeeman energy and the tension energy [21] does not change. The energy difference is mainly induced by the excessive dipolar energy. Changing the position of the bubble with a fixed radius on a disk is energetically the same as translation of the disk with fixed bubble position and radius. This situation is depicted in Fig. 3(d). Then, excessive magnetic surface charges are generated on both sides of the bubble with different distances. This asymmetry induced by

the distance difference produces the quadratic dependence of the energy on the disk shift Δx. After the calculation of the extra dipolar energy between these two magnetic surface charges and the bubble, we obtained the following asymptotic equation for the spring constant [25]:

$$\mathcal{K} \approx \frac{\mu_0 \pi M^2 d^2}{12 R_D}\left[\frac{48}{\tau} - 24\left(\frac{1}{\rho_-}+\frac{1}{\rho_+}\right) + \pi^2\left(1+\frac{2R_D^2}{d^2}\right)\left(\frac{1}{\rho_-}+\frac{13}{\rho_+}-\frac{14}{\tau}\right) + \frac{\pi^2 r}{R_D}\left\{\frac{1}{\rho_-^3}-\frac{13}{\rho_+^3}-\frac{2R_D^2}{d^2}\left(\frac{1}{\rho_-}-\frac{13}{\rho_+}\right)\right\}\right]. \quad (7)$$

Here, $\tau = \sqrt{1+(d/R_D)^2}$ and $\rho_\pm = \sqrt{(r/R_D \pm 1)^2 + (d/R_D)^2}$. In Fig. 3(c), we plotted the analytic line from Eq. (7), and it shows good agreement with the simulation results.

Using the $\mathcal{K}$ results, we compared the frequencies, respectively, derived from massless Thiele's equation [Eq. (1)] and the massive equation [Eq. (2)]. The massless equation produced only one frequency, $\omega = \mathcal{K}/\mathcal{G}$, plotted in Fig. 2. However, the massive equation generates two different frequencies: one with a positive value and one with a negative value. The positive ω_+ converges to ω at the low radius range. So, we can regard ω_+ as a perturbed frequency from ω. This is a reasonable expectation since the amount of perturbation increases as the bubble radius increases and the mass effect depends on the bubble radius. In contrast to ω_+, the ω_- of the massive equation is not a perturbed frequency from ω because the sign is opposite. The term ω_- is solely a nontrivial frequency originating from the mass term. These two frequencies also can be predicted from Eqs (5) and (7). These frequencies are plotted in Fig. 2 and are well matched to the simulation results. This means that we can expect the gyration motion with a given radius of the skyrmion bubble.

Finally, we point out the usefulness of a "regular polygon" trajectory for the skyrmion magnetic bubble experiments. In the vortex core gyration experiments with conventional in-plane material, a time-resolved experiment is needed for detecting the vortex gyration [1,2] because the gyration occurs within several nanoseconds and the trajectories resemble a circle. The time for bubble gyration is expected to be of the order of nanoseconds for one rotation, but the trajectories show hypocycloidal shapes, not circles. This difference makes it possible to detect the gyration of the bubble with non-time-resolved experiments. If we obtain an integer for the angular frequency ratio ω_-/ω_+ through the bubble radius adjustment using the external field, the time-averaged images show flowerlike patterns [Figs. 4(a)–4(c)]. This means that time-resolved experiments are not essential for measuring the bubble dynamics; therefore, we expect that the frequency-ratio-tuning method will be useful to detect the bubble gyration.

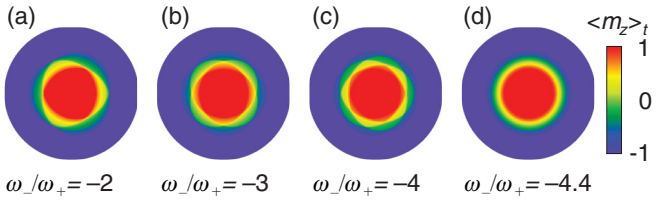

FIG. 4. (Color online) Time-averaged images of bubble gyrations. We assumed the zero wall width and neglected the damping effect. Different colors denote the time-averaged perpendicular magnetic component $\langle m_z \rangle_t$ during the bubble gyration. The angular frequency ratio ω_-/ω_+ is integers (a–c) and not integer (d).

IV. CONCLUSIONS

We studied the gyration of a skyrmion magnetic bubble numerically and analytically using a constant external field. The radius of the bubble was controlled systematically by the external field and determined the gyration of the bubble. Adjusting the external field, the bubble gyrations showed various polygonlike trajectories, including regular polygons with a natural number of vertices. Using the various polygonlike trajectories, the mass of the bubble and the spring constant were obtained and showed good agreement with the analytic calculation. This analytic formulation will be useful in further studies, including unconventional effect such as DMI. In addition, we suggested that the regular polygon trajectory is useful for the experiments of the skyrmion bubble gyration.

ACKNOWLEDGMENTS

This research was supported by the International Research and Development Program of the National Research Foundation of Korea (NRF) funded by the Ministry of Education, Science and Technology (MEST) of Korea (Grant No. 2012-00156, FY 2012).

[1] S.-B. Choe, Y. Acremann, A. Scholl, A. Bauer, A. Doran, J. Stöhr, and H. A. Padmore, Science **304**, 420 (2004).
[2] B. Van Waeyenberge, A. Puzic, H. Stoll, K. W. Chou, T. Tyliszczak, R. Hertel, M. Fähnle, H. Brükl, K. Rott, G. Reiss, I. Neudecker, D. Weiss, C. H. Back, and G. Schütz, Nature (London) **444**, 461 (2006).
[3] M.-Y. Im, P. Fischer, K. Yamada, T. Sato, S. Kasai, Y. Nakatani, and T. Ono, Nat. Commun. **3**, 983 (2012).
[4] S.-K. Kim, K.-S. Lee, Y.-S. Yu, and Y.-S. Choi, Appl. Phys. Lett. **92**, 022509 (2008).
[5] J. Miltat and A. Thiaville, Science **298**, 555 (2002).
[6] K. Yamada, S. Kasai, Y. Nakatani, K. Kobayashi, H. Kohno, A. Thiaville, and T. Ono, Nat. Mater. **6**, 270 (2007).
[7] A. A. Thiele, Phys. Rev. Lett. **30**, 230 (1973).
[8] O. A. Tretiakov, D. Clarke, G.-W. Chern, Y. B. Bazaliy, and O. Tchernyshyov, Phys. Rev. Lett. **100**, 127204 (2008).
[9] O. A. Tretiakov and O. Tchernyshyov, Phys. Rev. B **75**, 012408 (2007).

[10] C. Moutafis, S. Komineas, C. A. F. Vaz, J. A. C. Bland, T. Shima, T. Seki, and K. Takanashi, Phys. Rev. B **76**, 104426 (2007).
[11] X. Z. Yu, Y. Onose, N. Kanazawa, J. H. Park, J. H. Han, Y. Matsui, N. Nagaosa, and Y. Tokura, Nature (London) **465**, 901 (2010).
[12] G. D. Skidmore, A. Kunz, C. E. Campbell, and E. D. Dahlberg, Phys. Rev. B **70**, 012410 (2004).
[13] M. Hehn, K. Ounadjela, J. P. Bucher, F. Rousseaux, D. Decanini, B. Bartenlian, and C. Chappert, Science **272**, 1782 (1996).
[14] S. Komineas, C. A. F. Vaz, J. A. C. Bland, and N. Papanicolaou, Phys. Rev. B **71**, 060405(R) (2005).
[15] C. Moutafis, S. Komineas, and J. A. C. Bland, Phys. Rev. B **79**, 224429 (2009).
[16] I. Makhfudz, B. Krüger, and O. Tchernyshyov, Phys. Rev. Lett. **109**, 217201 (2012)
[17] A. N. Bogdanov and U. K. Rößler, Phys. Rev. Lett. **87**, 037203 (2001).
[18] A. N. Bogdanov and D. A. Yablonskii, Zh. Eksp. Teor. Fiz. **95**, 178 (1989) [Sov. Phys. JETP **68**, 101 (1989)].
[19] M. J. Donahue and D. G. Porter, *OOMMF User's Guide Version 1.0* (National Institute of Standards and Technology, Gaithersburg, MD, 1999).
[20] Y. Y. Dai, H. Wang, P. Tao, T. Yang, W. J. Ren, and Z. D. Zhang, Phys. Rev. B **88**, 054403 (2013).
[21] K.-W. Moon, J.-C. Lee, S.-G. Je, K.-S. Lee, K.-H. Shin, and S.-B. Choe, Appl. Phys. Express **4**, 043004 (2011).
[22] G. Tatara and H. Kohno, Phys. Rev. Lett. **92**, 086601 (2004).
[23] E. Saitoh, H. Miyajima, T. Yamaoka, and G. Tatara, Nature (London) **432**, 203 (2004).
[24] S.-W. Jung, W. Kim, T.-D. Lee, K.-J. Lee, and H.-W. Lee, Appl. Phys. Lett. **92**, 202508 (2008).
[25] It was assumed that the domain wall width is zero and there are only two magnetization states (up and down). We calculated the energy E induced by surface magnetic charges. The spring constant $\mathcal{K}$ is obtained from $E \approx (\mathcal{K}/2)(\Delta x)^2$